(NASA-CR-164372) RESEARCH ON SOLAR-WIND AND MAGNETOSPHERIC ELECTRIC FIELDS AND PLASMAS Final Report, 1 Oct. 1979 - 1 May 1981 (Texas Univ. at San Antonio.) 22 p HC A02/MF A01 CSCL 03B G3/92

N81-25996 THRU N81-25997 Unclas 42423

RESEARCH ON SOLAR-WIND AND MAGNETOSPHERIC ELECTRIC FIELDS AND PLASMAS

FINAL REPORT

Principal Investigator: James L. Burch

Period Covered: October 1, 1979 to May 1, 1981

Center for Applied Research and Technology
University of Texas at San Antonio
San Antonio, Texas 78285

NASA-GSFC Grant No. NSG-5418

I. Introduction

Work under this has focused on the phenomena of particle precipitation and ion convection at high latitudes and their response to variations in the interplanetary magnetic field (IMF). This research has involved the analysis of data from the Low Energy Electron Experiment and the Retarding Potential Analyzer/Drift Meter on Atmosphere Explorers C and D. Ancillary data on the IMF were obtained from the spacecraft Imp-J through the National Space Science Data Center.

The results of this work have been published in a series of papers which are discussed breifly in the paragraphs which follow. Reprints or preprints of the complete papers are attached as Appendix A. In the course of this research significant collaborative efforts were conducted with scientists at Rice University (P. H. Reiff and R. W. Spiro), the University of Texas at Dallas (R. A. Heelis, W. B. Hanson, and J. D. Winningham), and NASA-Marshall Space Flight Center (S.A. Fields).

II. IMF Changes and Polar-Cap Electric Fields and Currents

The results of this research were reported in an invited paper which was presented at the AGU Chapman Conference on "Magnetospheric Substorms and Related Plasma Processes" held at Los Alamos, New Mexico on October 9-13, 1978. The paper was published in the conference proceedings as follows:

> Burch, J. L., and R. A. Heelis, IMF changes and polar-cap electric fields and currents, in Dynamics of the Magnetosphere, S.-I. Akasofu (ed.), p. 47-62, D. Reidel, 1979.

This paper focused on phenomena in the earth's polar cap, defined as the region poleward of the auroral oval. The polar cap is connected magnetically to the solar wind, and it is generally true that currents flow easily between the two regions and that polar-cap electric fields and currents respond sensitively to variations in the IMF. The effects of the solar-magnetospheric X, Y, and Z components of the IMF have proved to be quite distinct. Strong southward components are associated with a larger polar cap and stronger electric fields and field-aligned currents. Strong northward components lead to a smaller polar cap and perhaps to the occasional appearance of sunward convection within it. Positive IMF B_y components intensify dawnside antisunward convection in the northern hemisphere and may displace the cusp convection "throat" toward dusk. Negative B_y components intensify duskside antisunward convection and may displace the northern-hemisphere throat toward dawn. These displacements and intensifications respond in the opposite sense in the southern hemisphere. Variations of the X-component induce interhemispheric asymmetries in polar-cap particle access and acceleration, both phenomena increasing significantly in the hemisphere for which the tail magnetic field and the IMF have X-components of opposite signs. See Appendix A for the complete paper.

III. Polar Cap Electron Acceleration Regions

This research, which was conducted in collaboration with R.A. Heelis of UTD and S. A. Fields of MSFC, investigated the characteristics of electron acceleration processes in the polar caps and the effects of the IMF on their

occurrence distribution. The results have been published in the Journal of Geophysical Research as follows:

Burch, J. L., S. A. Fields, and R. A. Heelis, Polar Cap electron acceleration regions, J. Geophys. Res., 84 p. 5863-5874, 1979.

In this study it was found that electron energy spectra and angular distributions within polar-cap acceleration regions are generally consistent with models of acceleration of auroral primaries and reflection of atmospheric secondaries by field-aligned electrostatic potential differences. However, localized strongly field-aligned fluxes are also observed at energies below the spectral peak. We have suggested that these transient beams of field-aligned low-energy electrons result from the acceleration of thermal electrons from within the acceleration regions and that this thermal electron population may be partially replenished by small pitch angle atmospheric secondary electrons.

The occurrence of the polar cap acceleration regions in the northern hemisphere is strongly correlated with IMF vectors which project into the (-X,+Z) sector of the solar-magnetospheric X-Z plane; that is, with northward "away" IMF polarities. For the complete paper see Appendix A.

IV. Cusp Proton Signatures and the Interplanetary Manetic Field

This research was performed in a joint effort with Drs. P. H. Reiff and K. W. Spiro of Rice University. The work was reported in a paper entitled "Cusp Proton Signatures and the Interplanetary Magnetic Field", which has now been published in the Journal of Geophysical Research. The reference for this paper is as follows:

Reiff, P. H., J. L Burch, and K. W. Spiro, Cusp Proton Signatures and the Interplanetary Magnetic Field", J. Geophys. Res., 85, 5997, 1980.

In previous research we have suggested that the variation of proton average energy with latitude in the cusp is an indicator of the means of particle entry into the magnetosphere. If magnetic merging is the principal means of particle entry, the proton average energy should fall with increasing invariant latitude; if diffusion is the principal means of particle entry, the average energy should first fall and then briefly rise as a function of latitude, showing a "V" signature. In addition, the cusp protons should occur on open field lines in the former and closed field lines in the latter case. Four hundred passes of the AE-D satellite were scanned for appropriate cusp passes during periods when IMP-J interplanetary or magnetosheath magnetic field data were available. Sixty passes fulfilled all criteria. Of these, roughly a third showed clear or likely merging-type energy dispersions; a third showed clear or likely V-type energy dispersions, and a third showed unclear or no energy dispersions. The results are strongly correlated with the IMF: the merging signatures were associated with southward IMF and the V-signatures were associated with northward IMF. Unclear or no dipersion cases were associated with unsteady or weakly northward IMF or with orbits unfavorable to observe the dispersion (perpendicular to the convection direction). If one accepts the electron anisotropy boundary as an (imperfect) indicator of the last closed

field line, then the cusp protons are typically on open field lines for southward IMF and on closed field lines for northward IMF. In addition, the presence of $\geq$ 3 keV electrons in the cusp is strongly correlated with V-dispersions and therfore with northward IMF. The full manuscript of this paper appears in Appendix A.

V. The Relationships Between High Latitude Convection Reversals and the Energetic Particle Morphology Observed by Atmosphere Explorer

This work which was performed with Drs. R. A. Heelis, J. D. Winningham, and W. B. Hanson of UTD, has been reported in a paper which has now been published in the Journal of Geophysical Research as follows:

Hellis, R. A., J. D. Winningham, W. B. Hanson, and J. L. Burch, The Relationships Between High Latitude Convection Reversals and the Energetic Particle Morphology Observed by Atmosphere Explorer, J. Geophys. Res., 85, 3315, 1980.

In this paper it is noted that simultaneous measurements of auroral zone particle precipitation and ion convection velocity show a consistent difference between the location of the poleward boundary of auroral particle precipitation and the ion convection reversal. The difference, of about 1.5° of invariant latitude, is such that some part of the antisunward convection lies wholly within the particle precipitation region. The nature of the convection reversals within the precipitation region suggests that in this region the convection electric field is generated on closed field lines that connect in the magnetosphere to the low latitude boundary layer.

VI. Cusp Region Particle Precipitation and Ion Convection for Northward Interplanetary Magnetic Field

This research has investigated the characteristic patterns of particle precipitation and ion convection which occur in the dayside cusp region during periods of strong northward IMF. Initial results have been reported in the following paper, which has been published in Geophysical Research Letters:

Burch, J. L., P. H. Reiff, R.W. Spiro, R. A. Heelis, and S. A. Fields, Cusp Region Particle Precipitation and Ion Convection for Northward Interplanetary Magnetic Field, Geophys. Res. Lett., 7, 393, 1980.

In this research it was found that data from Atmosphere Explorer D for periods of strong northward interplanetary magnetic field show the following characteristic behavior in the dayside magnetospheric cusp region. Engergy-time spectrograms of suprathermal positive-ion fluxes exhibit a characteristic "V" pattern as the spacecraft moves toward higher latitudes; that is, with the peak in the energy spectrum falling in energy and then rising again. Convection velocities follow this pattern closely with strong east-west flows (with antisunward components) occurring in the equatorward half of the "V" and significant sunward flows occuring in the poleward

half of the "V". These patterns can be understood qualitatively in terms of a model of ionospheric electric potential produced by the known dependence of Birkeland current densities on magnetic activity. The full paper is contained in Appendix A.

VII. AE-C Observations of Electric Fields Around Auroral Arcs

The large-scale features of the ionospheric convection pattern at high latitudes are quite well documented and understood. There are, however, significant variations in the observed ion drift in the auroral zone that are associated with discrete events in the energetic particles. In this research the ion drift signatures associated with discrete auroral particle events were investigated in detail. We have found that the electric field signature around auroral arcs in the ionosphere is quite reproducible and that the region of the magnetosphere that is magnetically connected to the discrete arcs must have both large and small areas in which adjacent flow regions are opposed to one another. This paper was presented at the Chapman Conference on the Formation of Auroral Arcs and wil appear in the published proceedings. A copy of the manuscript appears in Appendix A.

VIII. A Satellite Investigation of Energy Flux and Inferred Potential Drop in Auroral Electron Energy Spectra.

A predicted relationship between auroral electron energy flux (ε) and the inferred accelerating potential drop (V) for accelerated Maxwellian distributions has been derived by R. Lundin and I. Sandahl. This relationship ($\varepsilon \alpha V^2$) has been favorably tested with sounding rocket data for $eV/E_c >> 1$ (where E_c is the characteristic energy of the Maxwellian distribution). This research has utilized data from AE-D to extend these studies over the range $0.2 < eV/E_c < 5$ and for a wide range of latitudes and local times on both the night side and the day side. The results show good agreement with the full accelerated Maxwellian model. We have further derived an analytical approximation to which ε much better describes the data over the range $0.2 < eV/E_c < 3$ than does the $\varepsilon \alpha V^2$ approximation. Analyses of individual energy spectra suggest that the attitude of the inferred potential drop maximizes near to the center of inverted -V structures. This paper has been submitted to Geophysical Research Letters. A copy of the manuscript appears in Appendix A.

APPENDIX A

A SATELLITE INVESTIGATION OF ENERGY FLUX AND INFERRED POTENTIAL DROP IN AURORAL ELECTRON ENERGY SPECTRA

J. D. Menietti
J. L. Burch†
Department of Space Sciences
Southwest Research Institute
P. O. Drawer 28510
San Antonio, TX 78284

†Also, Division of Earth & Physical Science
University of Texas at San Antonio
San Antonio, TX 78285

Abstract

A predicted relationship between auroral electron energy flux (ε) and the inferred accelerating potential drop (V) for accelerated Maxwellian distributions has been derived by R. Lundin and I. Sandahl. This relationship ($\varepsilon \propto V^2$) has been favorably tested with sounding rocket data by Lundin and Sandahl for the limiting case of $eV/E_c >> 1$ (where E_c is the characteristic energy of the accelerated Maxwellian distribtuion) and by L. Lyons for a single inverted-V observed by the Injun 5 satellite. The study reported in this paper has utilized data from Atmosphere Explorer D to extend these studies over the range $.2 < eV/E_c < 5$ and for a wide range of latitudes and local times on both the nightside and the dayside. Our results show good agreement with the full accelerated Maxwellian model. We have further derived an analytical approximation to the electron energy flux which much better describes the data over the range $.2 < eV/E_c \lesssim 3$ than does the $\varepsilon \propto V^2$ approximation. In addition, analyses of individual energy spectra at small and large pitch angles through well-defined inverted-V structures suggest that the altitude of the inferred potential drop maximizes near the center of the inverted-V's.

Introduction

Models involving the acceleration of Maxwellian electron populations by magnetic-field-aligned potential drops have been applied with some success to observed auroral electron distribution functions (see, e.g., Evans, 1974). In the context of such models Lundin and Sandahl (1978) and Lyons et al (1979) found the total precipitating energy flux (ε) carried by accelerated primary auroral electrons to vary approximately as the square of the inferred potential drop ($\varepsilon \propto V^2$). Lundin and Sandahl (1978) and Fridman and Lemaire (1980) have both shown analytically that this proportionality is expected when the ratio eV/E_c (where E_c is the characteristic energy of the Maxwellian distribution) is sufficiently large and the altitude of the potential drop is sufficiently high. In practice this approximation holds over only a very narrow range of values of eV/E_c.

The purpose of this paper is threefold: (1) To report on an analytical approximation to the accelerated Maxwellian energy flux which is valid for all values of eV/E_c in the range $0 < eV/E_c \lesssim (\frac{B_o}{B_v} - 1)$, where B_o and B_v are the magnetic field strengths at the altitude of observation and the altitude of the potential drop, respectively; (2) To compare experimental data from Atmosphere Explorer D with this approximation; and (3) To infer from the data the altitude distribution of the assumed potential drops.

Analytical Approximation for Total Precipitating Energy Flux

As pointed out by Lundin and Sandahl (1978), the total downward energy flux carried by an isotropic Maxwellian electron population accelerated by a field-aligned electrostatic potential drop may be written,

$$\varepsilon = \pi \left(\frac{B_o}{B_v}\right) \int_0^{E_b} (E + eV) J(E) dE + \pi \int_{E_b}^{\infty} \frac{(E + eV)^2}{E} J(E) dE \qquad (1)$$

where, $E_b = \dfrac{eV}{\left(\frac{B_o}{B_v} - 1\right)}$, and

$$J(E) = \frac{n}{2\pi^{3/2}} \left(\frac{2}{m}\right)^{\frac{1}{2}} \frac{E}{E_c^{3/2}} \exp(-E/E_c).$$

In this expression, m and n are the electron mass and density, respectively; while B_o, B_V, and V are as defined in the previous section. The significance of E_b is that it is the minimum pre-acceleration energy for which some magnetic reflection occurs at or above the altitude of observation. All electrons with initial energies below E_b which enter the region of the potential drop from above are still moving downward at the point of detection and hence contribute to ε. Equation (1) integrates to,

$$\varepsilon = K E_c \left[\frac{B_o}{B_V} (2E_c + eV) - \left| \frac{B_o}{B_V} eV + 2\left(\frac{B_o}{B_V} - 1\right)E_c \right| e^{-E_b/E_c} \right] \qquad (2)$$

where,

$$K = \frac{n}{2\pi^{1/2}} \left(\frac{2}{m}\right)^{\frac{1}{2}} \left(\frac{1}{E_c^{1/2}}\right).$$

Wherever $E_b < E_c$, the exponential term in Equation (2) can be approximated by the first two terms of the series $e^{-x} = 1 - x + x^2/2! - \ldots$, yielding,

$$\varepsilon \simeq K \left[\frac{R}{R-1} (eV)^2 + 2eVE_c + 2E_c^2 \right] \qquad (3)$$

where, R is the magnetic field ratio, $R = \frac{B_o}{B_V}$.

For $\frac{B_o}{B_V} >> 1$, eq. (3) becomes,

$$\varepsilon \simeq K \left[(eV)^2 + 2eVE_c + 2E_c^2 \right]. \qquad (4)$$

The condition $E_b < E_c$ means that eqs. (3) and (4) are valid approximations for all values of the ratio eV/E_c which do not approach or exceed the quantity $\left(\frac{B_o}{B_V} - 1\right)$. For this reason, eqs. (3) and (4) should be of much greater use than the approximation $\varepsilon \propto V^2$, particularly since typical values of eV/E_c are in the range $0 < eV/E_c < 5$ (Lin and Hoffman, 1979; Evans, 1974) while typical values of the quantity $\left(\frac{B_o}{B_V} - 1\right)$ are between 2.5 and 6 (for an observing altitude of 600 km and acceleration altitudes of 0.5 and 1.0 R_E, respectively). The fact that the range over which the $\varepsilon \propto V^2$ approximation is valid ($1 << eV/E_c < \left(\frac{B_o}{B_V} - 1\right)$) is exceedingly small has been pointed out previously by Fridman and Lemaire (1980).

More useful expressions are obtained by multiplying both sides of eqs. (3) and (4) by $E_c^{\frac{1}{2}}/nV^2$ obtaining in the case of eq. (4),

$$\frac{\epsilon E_c^{\frac{1}{2}}}{nV^2} = k \left[1 + 2 \frac{E_c}{eV} + 2 \left(\frac{E_c}{eV}\right)^2 \right]. \qquad (5)$$

In eq. (5) the parameter k is the same proportionality constant used by Lundin and Sandahl (1978) in their equation (7). Eq. (5) allows a wide range of experimental data to be compared with a single analytical approximation since the right-hand side depends only on the ratio E_c/eV and not on the specific values of n, E_c, and V for each measured distribution function.

A graphical comparison of eq. (2), eq. (5), and the approximation $\epsilon = kV^2$ is made in Figure 1 for the case where R = 4. In fact, as noted by Yeh and Hill (1980) eq. (2) is only weakly dependent on R in the range of eV/E_c values plotted in Figure 1. It is clear from Figure 1 that eq. (5) is a much better approximation than $\epsilon = kV^2$, particularly over the range $(eV/E_c)<3$. Also evident from Figure 1 is the fact that the validity of eq. (5) extends well above the limit $(E_b/E_c) = 1$ (i.e., $\frac{eV}{E_c} = 3$) below which the approximation $e^{-x} = 1-x$ is valid. This increased range of validity of eq. (5) results from the fact that the exponential (or second) term in eq. (2) is dominated by the first term for large values of eV/E_c.

Atmosphere Explorer Observations

Data from the Low Energy Electron Experiment (Hoffman et al, 1973) on Atmosphere Explorer D (AE-D) were analyzed to assess the extent to which experimental auroral electron observations can be described by accelerated Maxwellian distributions and the various models of Figure 1. A set of 10 orbits (5 dayside and 5 nightside) were chosen for analysis based on the significant occurrence of inverted-V type electron precipitation. The slow spin rate (20 rpm) of AE-D causes excessive spatial aliasing in the full angular distributions obtained during spinning orbits.

Attention was therefore confined to non-spinning orbits and the -7° and 60° electron analyzers (Hoffman et al, 1973), each of which sampled complete energy spectra once per second. From these orbits, which occurred from November 1975 through early January 1976, 455 electron spectra were fit to accelerated Maxwellian distributions (Evans, 1974). Of the total set of 455 energy spectra, 160 were fit sufficiently well by the accelerated Maxwellian to be considered further. The others were generally either unaccelerated Maxwellian distributions or did not produce good fits due to spatial aliasing. For reference the distribution in invariant latitude and magnetic local time of the locations of the 160 electron spectra well characterized by accelerated Maxwellian distributions is plotted in Figure 2. The altitudes of the observations varied from 200 km to 800 km.

An example of the electron energy spectra measured by the -7° and 60° detectors (crosses and circles, respectively), along with the accelerated Maxwellian fit to the -7° data are shown in Figure 3. Noted on Figure 3 are the model parameters, which include the electron density (n), the Maxwellian characteristic energy (E_c), and the potential drop multiplied by the electron charge (eV). A characteristic feature seen in Figure 3 is the non-Maxwellian high-energy tail of the electron energy spectra.

The primary electron beam, consisting of particles which have been accelerated through the complete potential drop, are those with $E \geq 2.26$ keV in Figure 3. Electrons with lower energies may be trapped secondaries as postulated by Evans (1974). Within the primary beam there typically exists a transition energy (~8 keV in Figure 3) above which the electrons are isotropic or peaked slightly at large pitch angles. At energies below the transition energy field-aligned fluxes are observed. In the notation of the previous section this transition energy is given by $E_T = E_b + eV$, and is related to the ratio B_O/B_V as follows,

$$R = \frac{B_O}{B_V} = \sin^2\alpha_{60}\ E_T/(E_T-eV), \qquad (5)$$

where α_{60} is the pitch angle sampled by the 60° detector. As described by Evans (1974), E_T can be used to estimate the altitude of the

inferred potential drop, or equivalently the ratio B_o/B_v as a simple consequence of conservation of the first adiabatic invariant.

Comparison of Data with Model Approximations

For all 160 electron spectra the parameters, E_c, and eV were derived from a least squares fit of an accelerated Maxwellian distribution to the small pitch-angle (-7° detector) data as shown in Figure 3. Also, n and the total downward energy flux (ε) were determined from the experimental data for $E \geq eV$, without regard to the model fit, by assuming an isotropic energy flux equal to the average of the -7° and 60° energy fluxes. In the bottom of panel of Figure 4 the quantity $\varepsilon E_c^{\frac{1}{2}}/nV^2$ is plotted versus the ratio eV/E_c. Dayside data are plotted as solid circles, while nightside data appear as crosses.

As predicted by the accelerated Maxwellian model, the AE-D data are well ordered by the two parameters plotted in Figure 4. Also evident is the concentration of data points in the range $0.5 \lesssim eV/E_c \lesssim 3$, over which the approximation of eq. (5) has its highest validity (see Figure 1). Plotted for reference in Figure 4 are eq. (2) (with an assumed value R = 4) and the approximation $\varepsilon E_c^{\frac{1}{2}}/nV^2 = k$.

If the measured electron populations were perfect accelerated Maxwellian distributions all the data points in the lower panel of Figure 4 would lie along the solid curve (eq. 2). Although some uncertainty results from the lack of complete pitch-angle coverage, the primary reason that the data points lie significantly above the eq.(2) curve is the existence of the high-energy tails as shown in Figure 3. Since the high-energy tail appears in all cases and contributes substantially to the total energy flux, a valid model of the auroral acceleration mechanism must account for it. Figure 1 shows that as eV/E_c increases, the approximation of eq. (5) actually becomes a better representation of the total energy flux than the full eq. (2). It is also evident in Figure 4 that the effect of the high-energy tail is of the same magnitude for dayside and nightside observations.

Altitude Distribution of Inferred Potential Drops

Eq. (5) has been used to estimate the ratio $R = B_o/B_V$ for all 160 data points in the bottom panel of Figure 4. The results are plotted in the upper panel of Figure 4, again with solid circles for dayside and crosses for nightside observations. There is a clear tendency, particularly in the nightside data, for B_o/B_V to increase as the ratio eV/E_c increases. In addition, high values of B_o/B_V ($\gtrsim 4$) occur for significantly lower eV/E_c ratios for the dayside data than for the nightside data. Most notable in Figure 4, however, is the large amount of scatter in the B_o/B_V values. In an attempt to identify an ordering parameter for B_o/B_V, both E_c and eV were examined individually but with negative results. However, when individual inverted-V structures were examined there emerged a clear tendency for the higher B_o/B_V ratios to occur near the center of each inverted-V. Of the 160 observations in Figure 4, 45 occurred through well-defined inverted-V structures. For these 45 observations, the B_o/B_V ratio was compared to the ratio V/V_{max}, where V_{max} is the maximum inferred potential drop for a particular inverted-V. The results, which appear in Figure 5 suggest a strong tendency for higher B_o/B_V values (higher altitude potential drops), to occur near the center of the inverted-V's with lower B_o/B_V values near their edges.

Discussion

We have shown that the expression for integrated energy flux carried by an accelerated Maxwellian electron distribution (Lundin and Sandahl, 1978) is a good representation of the actual data from AE-D over the range $0 < eV/E_c < 5$. We have derived equation (3) (our approximation to equation (1)) which holds for a much wider interval ($0 < eV/E_c < R-1$) than the Lundin-Sandahl approximation $\varepsilon \propto kV^2$. We have tested many different values of the B-ratio, R, ranging from 1 to over 100 (an altitude range of 0 to ~ 3.7 Re) and found the shape of the curves for equations (1) and (3) as represented in Figures 1 and 4 are essentially the same. There is very little dependence of ε on R over the range $0 < eV/E_c < 5$. This is in agreement with the work of Fridman and Lemaire (1980). Finally, by noting the transition energy or energy at which the electron flux becomes isotropic or slightly peaked at large pitch

angles we calculated the B-ratio from the first adiabatic invariant. Two points of interest can be made. First there appears to be a greater number of nightside high B-ratio values for larger eV/E_c as shown in the upper panel of Figure 4. By replotting the calculated B-ratios versus a normalized potential, V/V_{max}, we have discovered that the centers of the inverted-V potential contours appear to be located at higher altitude than do the edges. From Figure 5, if we assume the range of B-ratios for a typical inverted-V event is $\sim$3.5, this corresponds to an altitude extent of $\sim$.8 Re. We are not suggesting that our analyses preclude double-layers (which have very small radial extent), but our results do warrant a more careful investigation of other data sets possibly utilizing other procedures for determining the radial extent of the inverted-V electron acceleration mechanism.

Acknowledgements

We would like to thank Faye Whitaker and Angel O'Campo for their assistance (many long hours) at the computer terminal. This work was supported by NASA Grant NSG5418, NSF Grant ATM78-26762, and the SwRI Internal Research Program.

References

Evans, David S., Precipitating Electron Fluxes Formed by a Magnetic Field Aligned Potential Difference, J. Geophys. Res., 79, 2853-2858, 1974.

Fridman, M. and Lemaire, J., Relationship Between Auroral Electron Fluxes and Field Aligned Electric Potential Difference, J. Geophys. Res., 85, 664-670, 1980.

Hoffman, R. A., Burch, J. L., Janetzke, R. W., McChesney, J. F., Way, S. H., and Evans, D. S., Low Energy Electron Experiment for Atmosphere Explorer-C and -D, Radio Sci., 8, 393-400, 1973.

Lin, C. S., and Hoffman, R. A., Fluctuations of Inverted V Electron Fluxes, J. Geophys. Res., 84, 6547-6553, 1979.

Lundin, R. and Sandahl, I., Some Characteristics of the Parallel Electric Field Acceleration of Electrons Over Discrete Auroral Arcs as Observed From Two Rocket Flights, Proceedings of Esrange Symposium, Ajaccio, 24-29 April 1978 (ESA SP-135, June 1978).

Lyons, L. R., Evans, D. S., Lundin, R., An Observed Relation Between Magnetic Field Aligned Electric Fields and Downward Electron Energy Fluxes in the Vicinity of Auroral Forms, J. Geophys. Res., 84, 457-461, 1979.

Yeh, H.-C. and Hill, T. W., Mechanism of Parallel Electric Fields Inferred From Observations, submitted to J. Geophys. Res. Dec. 23, 1980.

FIGURE CAPTIONS

Figure 1. The rearranged equation (2) (no-approximation expression) and equation (5) (our approximation) are plotted versus eV/E_c. Note the close agreement over the range $.2 < eV/E_c < 3$ for the case $B_o/B_V = 4$. Also shown is the "Lundin constant", k (dot-dash line).

Figure 2. Data sampling locations in magnetic local time and invariant latitude for the 160 data points used in this study.

Figure 3. Sample spectral plot of particle flux, J, versus energy for the -7° electron analyzer (+) and the +60° electron analyzer (o). The solid curve is a least squares fit to an accelerated Maxwellian for the primary electron population (E >2.26 keV). The points for E <2.26 keV are the postulated secondary backscattered electrons. Note also the high energy "tail" for E > 10 keV on this curve. At E~8 keV the fluxes for both electron analyzers become equal. This energy is referred to as the transition energy in the text.

Figure 4. (Lower panel) This figure is the same as Figure 1 except now the 160 data points are also included (· = dayside pts; x = nightside pts). ε and n are in cgs units, E_c is in keV and V is in kV. For this figure also, $B_o/B_V = 4$. (Upper panel) The B-ratio is plotted versus eV/E_c (· = dayside pts; x = nightside pts).

Figure 5. The B-ratio is plotted versus V/V_{max} where V_{max} is the maximum potential for a particular inverted-V electron precipitation event. A total of 45 points are included in this plot. The error bars designate the standard deviation of each set of points.

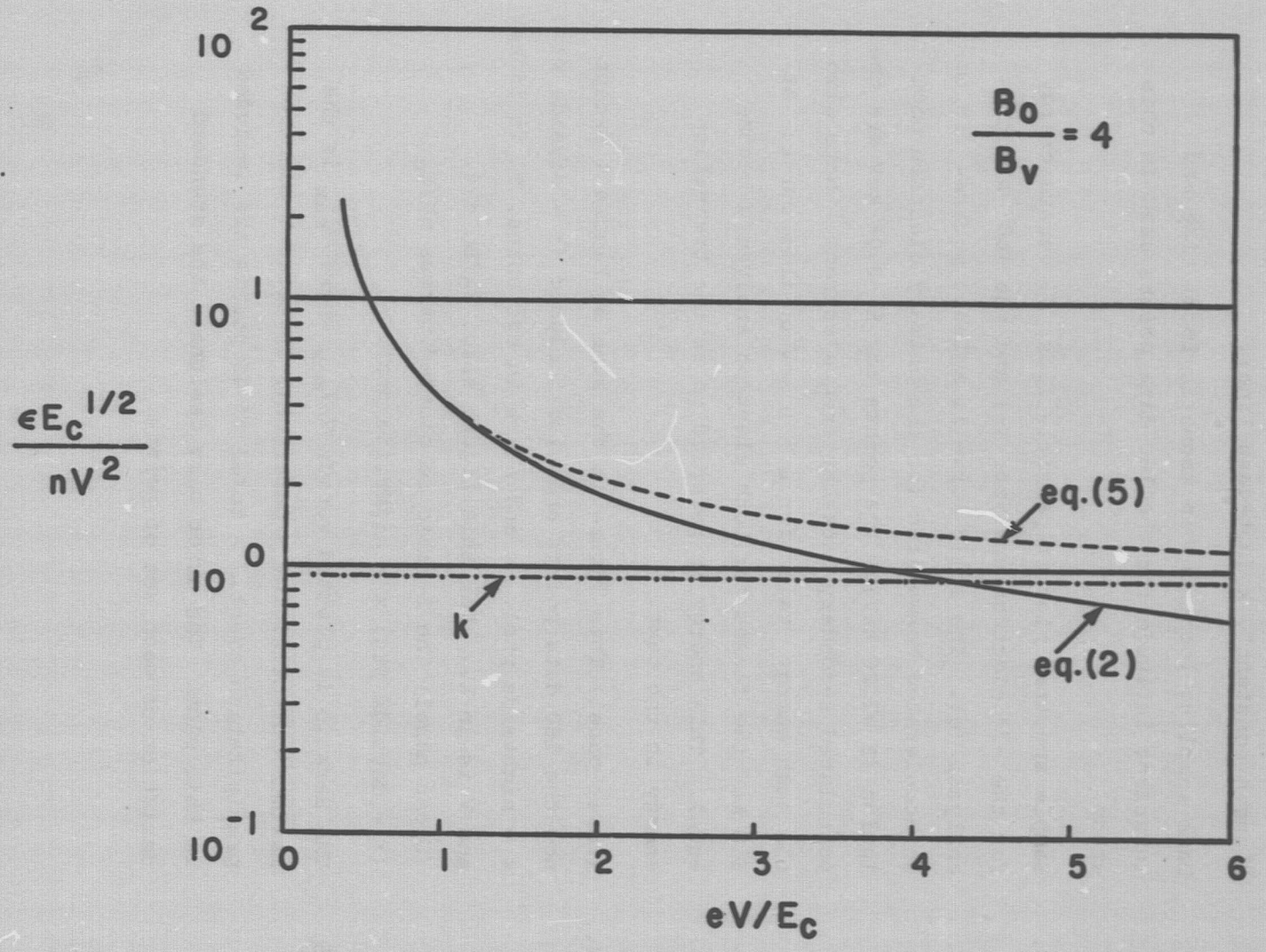
$\frac{B_0}{B_v} = 4$
eq.(5)
eq.(2)
k
$\frac{\epsilon E_c^{1/2}}{nV^2}$
eV/E_c
10^2
10^1
10^0
10^{-1}
0
1
2
3
4
5
6

FIGURE 1

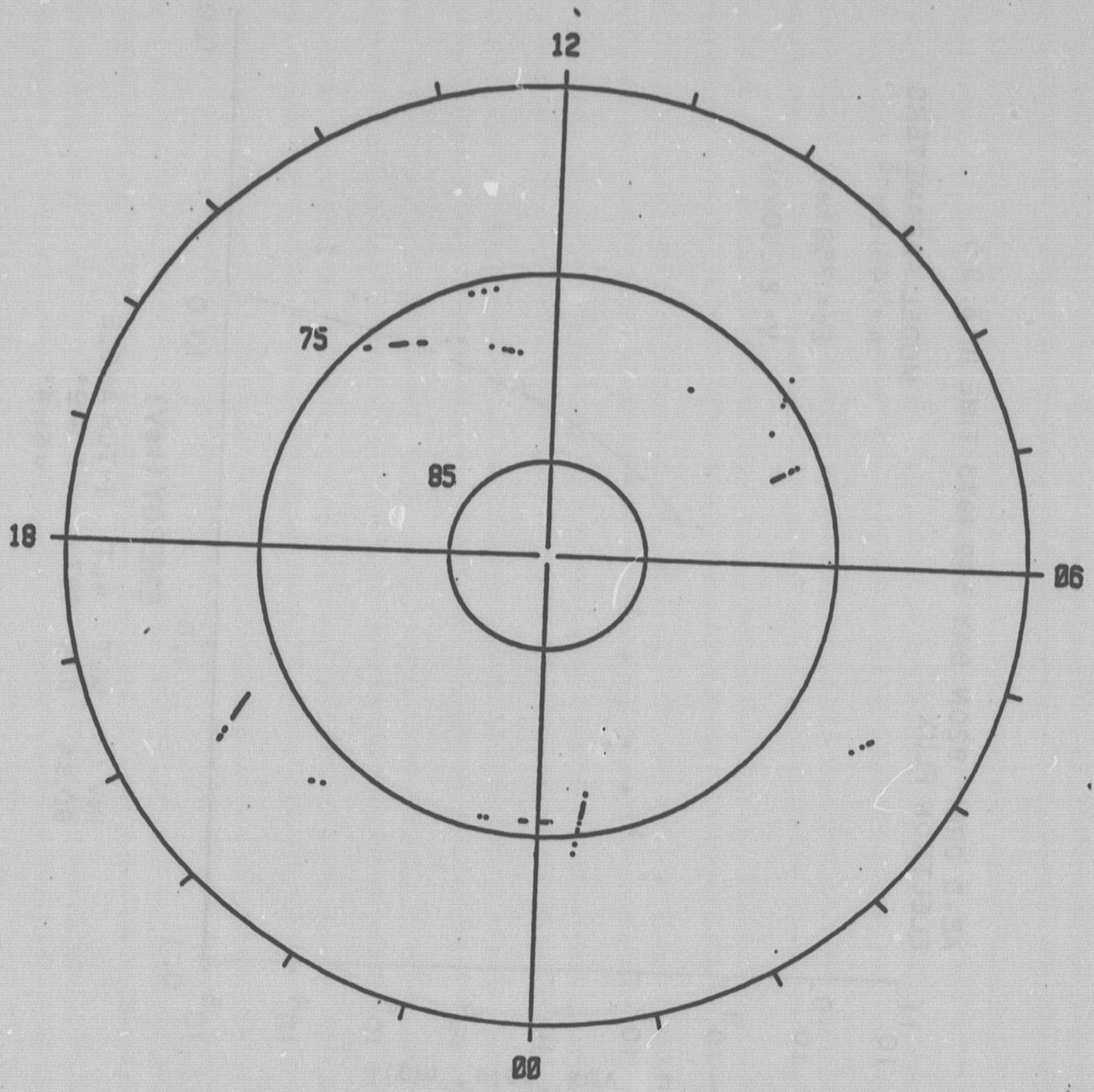

FIGURE 2

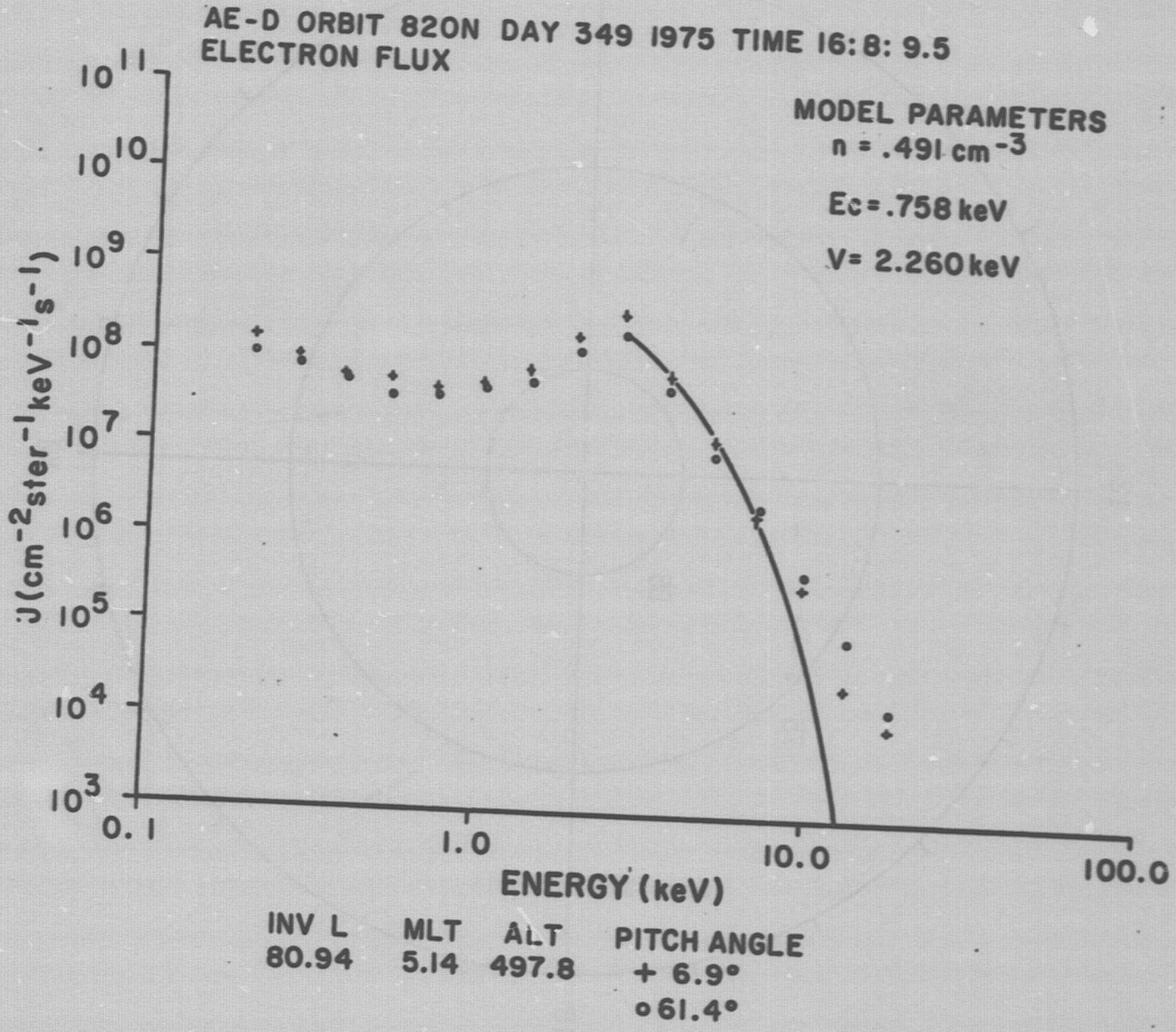
AE-D ORBIT 820N DAY 349 1975 TIME 16:8: 9.5
ELECTRON FLUX
MODEL PARAMETERS
n = .491 cm⁻³
Ec = .758 keV
V = 2.260 keV
J(cm⁻²ster⁻¹keV⁻¹s⁻¹)
10¹¹
10¹⁰
10⁹
10⁸
10⁷
10⁶
10⁵
10⁴
10³
0.1
1.0
10.0
100.0
ENERGY (keV)
INV L
80.94
MLT
5.14
ALT
497.8
PITCH ANGLE
+ 6.9°
○ 61.4°

FIGURE 3

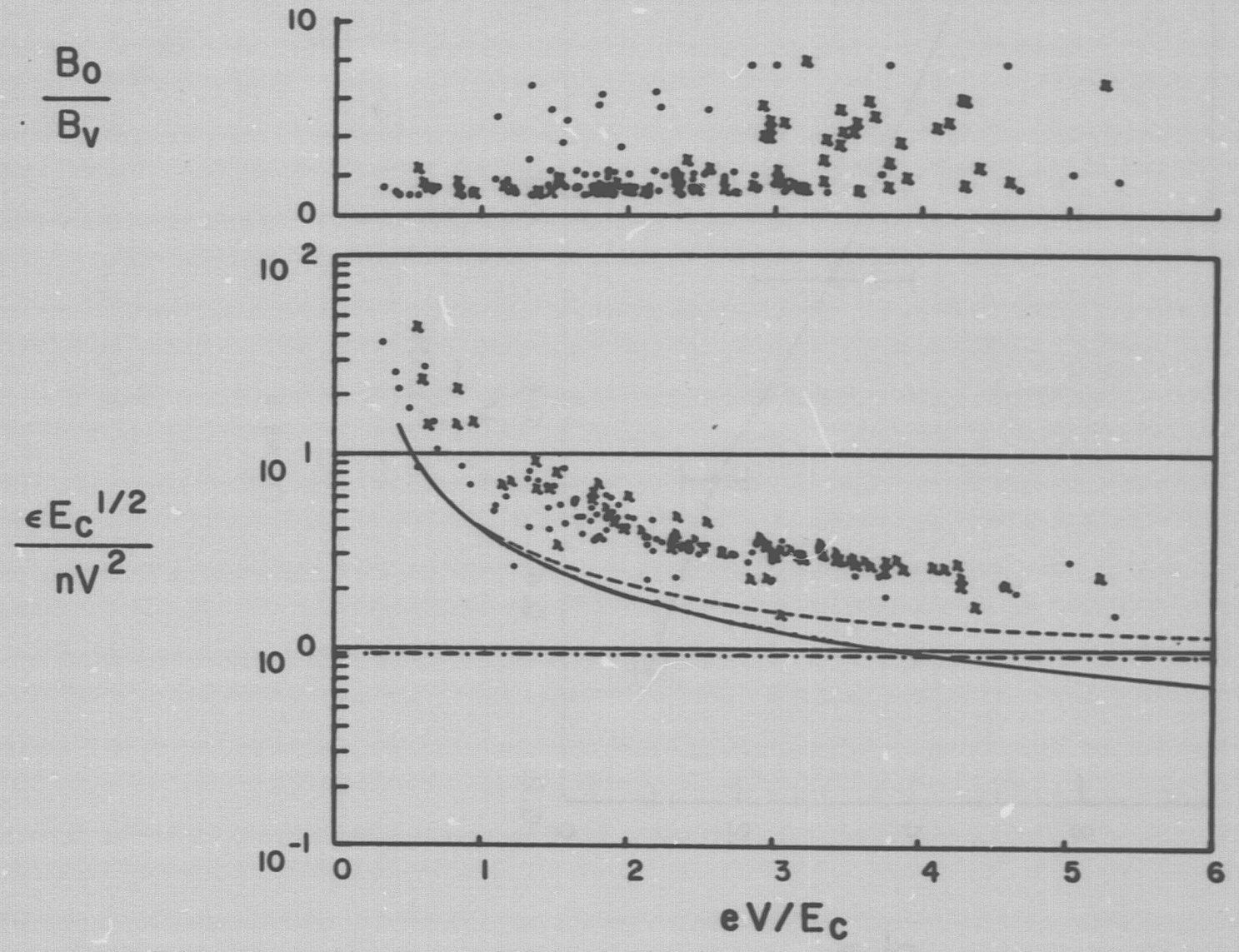
$\frac{B_0}{B_V}$
10
0
$\frac{\epsilon E_c^{1/2}}{nV^2}$
10^2
10^1
10^0
10^{-1}
0
1
2
3
4
5
6
eV/E_c

FIGURE 4

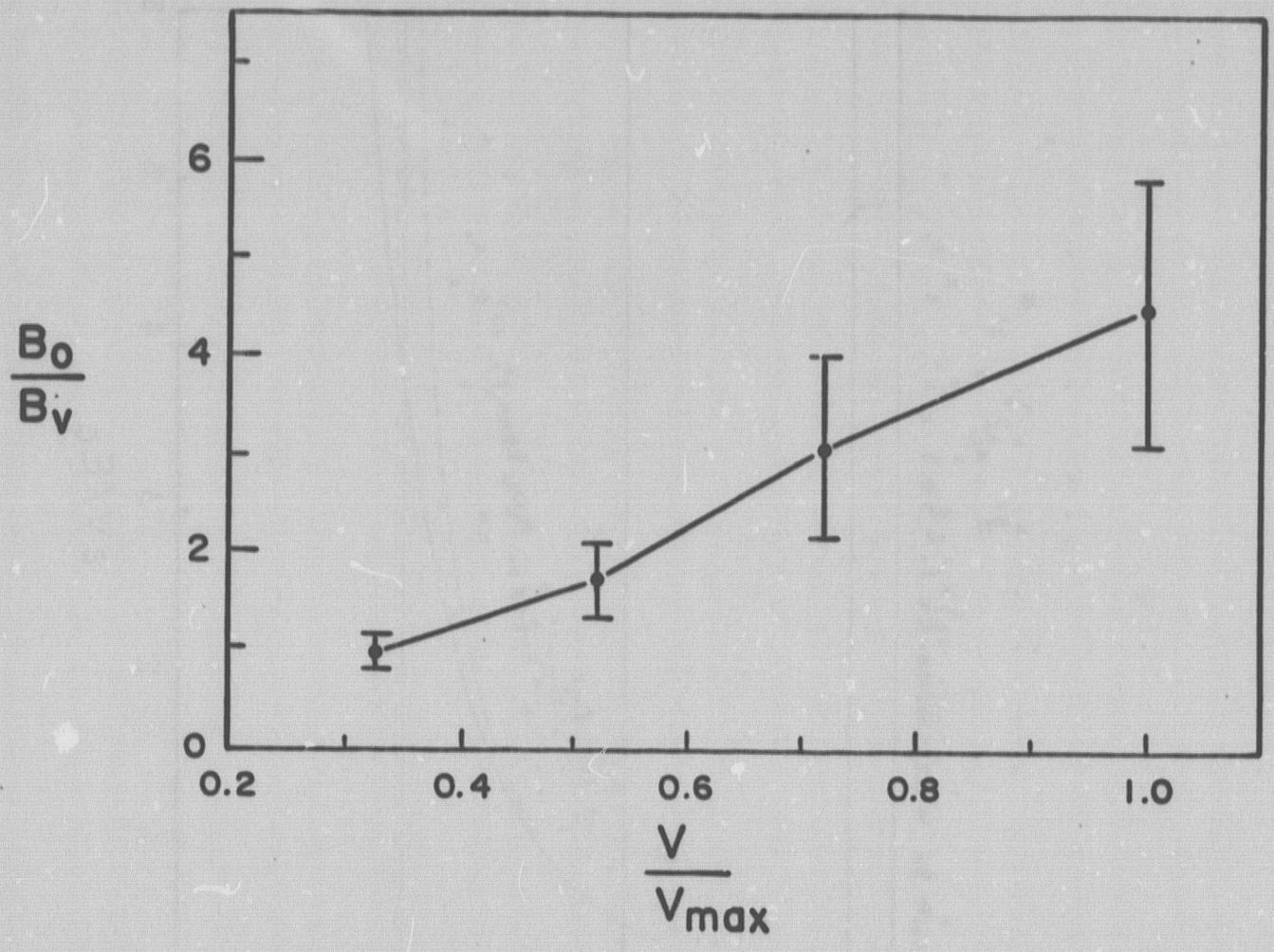

FIGURE 5